J Low Temp Phys (2007) 149: 185–199
DOI 10.1007/s10909-007-9507-6

Magnetotransport Properties and Mechanism of the A-Site Ordering in the Nd–Ba Optimal-Doped Manganites

S.V. Trukhanov · A.V. Trukhanov · H. Szymczak · C.E. Botez · A. Adair

Received: 14 November 2006 / Revised: 25 May 2007 / Published online: 24 August 2007

Abstract The crystal structure and magnetotransport properties of the $Nd_{0.70}Ba_{0.30}$-$MnO_{3.00-\delta}$ manganites have been investigated. The stoichiometric A-site ionic disordered $Nd_{0.70}Ba_{0.30}MnO_{3.00}$ sample is orthorhombic (SG = Imma) ferromagnet below $T_C \approx 151$ K. It has metal-insulator transition at $T_{MI} \approx 140$ K and peak of magnetoresistance ∼50% in field of 9 kOe. The anion-deficient partly A-site ionic ordered $Nd_{0.70}Ba_{0.30}MnO_{2.60}$ sample is ferrimagnet with $T_N \approx 130$ K and has nanometric ∼440 nm grains. The oxygen annealed stoichiometric partly A-site ordered $Nd_{0.70}Ba_{0.30}MnO_{3.00}$ sample consists of two perovskite phases: (i) A-site ionic completely ordered tetragonal (SG = P4/mmm) $NdBaMn_{2.00}O_{6.00}$ with a Curie point of ∼310 K and (ii) superstoichiometric orthorhombic (SG = Pnma) $NdMnO_{3.00+\gamma}$ with a Curie point of ∼120 K. The magnetoresistance of this sample at the room temperature is about 7% in a field of 9 kOe. Considerable changes of the magnetic properties are interpreted as due to the ordering of Nd^{3+} and Ba^{2+} cations as well as the formation of nanometric grains.

Keywords A-site ionic ordering · Manganites · Crystal structure · Magnetic ordering

PACS 75.30.Et · 75.30.Vn · 75.50.Lk

S.V. Trukhanov (✉)
The Joint Institute of Solids and Semiconductor Physics, NAS of Belarus, P. Brovka str. 19, 220072 Minsk, Belarus
e-mail: truhanov@ifttp.bas-net.by

A.V. Trukhanov
The Chemistry Department, Vitebsk State University, Moscow av. 33, 210036 Vitebsk, Belarus

H. Szymczak
The Institute of Physics, PAS, Lotnikov str. 32/46, 02-668 Warsaw, Poland

C.E. Botez · A. Adair
The University of Texas at El Paso, El Paso, TX 79968-0515, USA

1 Introduction

The A-site ordered perovskites $LBaB_2O_{6-\gamma}$ (L = La, Pr, Nd, Sm, Eu, Gd, Tb, Y; B = Mn, Co; $0 \leq \gamma \leq 1$) have been synthesized and thoroughly investigated by several groups [1–15]. The exploration of these layered perovskites has revealed the strong electron correlations and coupling between spin, charge, orbital, and lattice degrees of freedom which stimulates a renewed interest for these challenging materials. It has been established that the orbital physics phenomena, magnetic and electronic states in these compounds are derivatives from the ionic, orbital and charge ordering, nanoscopic phase separations, changes in the spin state of Co ions, a "spin blockade" mechanism and so forth.

The layered $LBaMn_2O_{6-\gamma}$ manganites have been found to possess unique physical properties, which are related to the ordering of cations on the A-sublattice of the perovskite structure [5–15]. The main structural feature of these A-site ordered compounds is the alternation of MnO_2 planes with two other planes LO and BaO, each containing cations of one type which results in a periodic distortion of MnO_6 octahedra. This crystal structure is similar to that of $YBaCuFeO_5$ [16]. The physical properties of such A-site ordered $LBaMn_2O_6$ manganites [17–26], cannot be explained taking into account the tolerance factor alone, as in the case of a statistical distribution of substituent cations in manganites of the $L_{0.50}Ba_{0.50}MnO_3$ type. This type of cation ordering increases the temperature of the phase transition from a metallic ferromagnetic state to an insulating paramagnetic state. In the case of $L^{3+} = Pr^{3+}$ the Curie temperature increases from ∼140 K to ∼320 K [27]. In both the disordered and ordered cases, the MR effect is observed at temperatures slightly below T_C.

For the manganites with $L^{3+}/Ba^{2+} = 1/1$ it has been established that the various degrees of L/Ba disorder on the A-sites may be realized [28, 29]. The magnetic ground state is a mixture of the ferromagnetic metallic (FM) and antiferromagnetic insulator (AFI(CE-type)) phases for the fully A-site ordered $LaBaMn_2O_6$ while the antiferromagnetic metallic (AFM(A-type)) one for the fully A-site ordered $PrBaMn_2O_6$ and $NdBaMn_2O_6$ [30]. The $[Pr_gBa_{1-g}]_P[Pr_{1-g}Ba_g]_BMn_2O_6$ compounds with various degrees of A-site order have been synthesized from the fully A-site ordered $PrBaMn_2O_6$ by controlling the annealing time and temperatures (1273–1623 K) in O_2 flow [28]. The A-site disorder gradually suppresses the antiferromagnetic interactions and the fully A-site disordered $Pr_{0.50}Ba_{0.50}MnO_3$ sample has a FM ground state. In previous studies [7, 31] the FM ground state for the A-site ordered $LaBaMn_2O_6$ and $NdBaMn_2O_6$ samples has been revealed that be connected with the partly A-site ordering.

Recently, the manganites with $L^{3+}/Ba^{2+} \neq 1/1$ cation ratio have been investigated [32, 33]. The ferromagnetic properties have been observed for the A-site ordered $La_{1-x}Ba_xMnO_3$ samples with $x = 0.44$ and 0.48. The ferromagnetic and antiferromagnetic properties have been observed for the sample with $x = 0.52$. For the $x = 0.50$ sample, neutron powder diffraction data provide evidence for a structural phase separation below 180 K and a stable and complex antiferromagnetic charge ordered phase at temperatures below ∼120 K. Contrary to previous reports, this charge ordered phase is not of the charge exchanged type and is not intrinsic to the main high temperature ferromagnetic phase. For the $x = 0.52$ sample, a similar charge ordered

state has been observed within a narrow temperature range at ∼180 K before it disappeared in favor of a more stable antiferromagnetic A-type orbital ordered phase [33].

Therefore, it is very interesting to study the mechanism of the A-site ordering and magnetic properties of the manganites with $L^{3+}/Ba^{2+} \gg 1$ cation ratio. In the present paper we have selected the $Nd_{0.70}Ba_{0.30}MnO_3$ solid solution. It is shown that the A-site ordering in this manganite results from the nanoscale chemical phase separation on the Ba-enriched and Ba-depleted regions.

2 Experimental Methods

The starting A-site disordered $Nd_{0.70}Ba_{0.30}MnO_{3.00}$ manganites have been obtained from high purity oxides and carbonate: Nd_2O_3, Mn_2O_3 and $BaCO_3$. At first the oxides and carbonate have been mixed to obtain desired (Nd^{3+}:Ba^{2+}:Mn^{3+} = 7:3:10) cation ratio and ground thoroughly in an agate mortar by adding some quantity of ethyl alcohol. Then the prefiring has been performed at 1000 °C in air during 2 h to remove a moisture and carbonic acid. The final synthesis has been carried out at 1400 °C in air during 2 h. After the synthesis the samples have been slowly cooled (100 °C/h) in order to receive the stoichiometric oxygen content. The air-prepared $Nd_{0.70}Ba_{0.30}MnO_3$ samples have been treated in an evacuated and sealed silica tubes at 800 °C for 24 h using Ta as oxygen getter to reduce the oxygen content to "$O_{2.60}$":

$$Nd_{0.70}Ba_{0.30}MnO_{3.00} + 0.16Ta \longrightarrow Nd_{0.70}Ba_{0.30}MnO_{2.60} + 0.08Ta_2O_5. \quad (1)$$

The oxygen-deficient sample is characterized by the partial ordering of Nd^{3+} and Ba^{2+} cations and the pyramidal Mn^{2+}/Mn^{3+} layers, sandwiched between alternating Nd^{3+} oxygen-free and Ba^{2+} oxygen-filled layers along the c axis. To lower a relative error of oxygen content measurements the weight of the sample placed in the silica tube has been ∼3 g. The anion-deficient partly A-site ordered $Nd_{0.70}Ba_{0.30}MnO_{2.60}$ sample has been oxidized in air at 800 °C during 12 h up to the oxygen-stoichiometric "O_3" state, where the partial A-site ordering remains:

$$Nd_{0.70}Ba_{0.30}MnO_{2.60} + O_2 \longrightarrow Nd_{0.70}Ba_{0.30}MnO_{3.00}\ (PO). \quad (2)$$

The microstructure of all samples has been studied by a NANO LAB-7 scanning electron microscope. The quantitative chemical content and its spatial distribution have been examined by the MS-46 and SYSTEM-860-500 microprobes. These investigations have shown that all samples are well crystallized with homogeneous chemical content. The oxygen content of all the products has been determined by thermogravimetric analysis. Thus, the chemical formula for all the examined samples may be written as $Nd_{0.70}Ba_{0.30}MnO_{3.00-\delta\pm0.01}$. X-ray powder diffraction data have been recorded at room temperature with a DRON-3M diffractometer in Cu–K_α radiation in angle range $20° \le 2\theta \le 80°$. The X-ray diffraction patterns have been analyzed by the Rietveld method [34] using the FullProof software [35]. The data have been collected with 0.03° step during the 3 s.

The magnetization measurements have been made using an SQUID-magnetometer in the temperature range 4.2–350 K. The temperature dependences of the specific

magnetization have been measured in a field of 100 Oe field during heating after zero-field cooling (ZFC) and field cooling (FC) mode. The field dependences have been also measured at low temperature (20 K) to avoid the magnetic contribution of the Nd^{3+} cations. The magnetic ordering temperature (T_C or T_N) has been defined as an inflection point of the ZFC magnetization measured in 100 Oe. The resistivity was studied from 77 to 350 K using a standard four-point-probe technique and with ultrasonically applied indium eutectic contacts. The negative isotropic MR is defined as:

$$MR = [\rho(H) - \rho(0)]/\rho(0) \times 100\%, \tag{3}$$

where $\rho(H)$ and $\rho(0)$ are the resistivities measured in a magnetic field of $H = 9$ kOe and in the absence of an applied magnetic field.

3 Experimental Results and Discussion

The microstructure investigations have shown that the as-prepared $Nd_{0.70}Ba_{0.30}MnO_{3.00}$ sample has well crystallized grains with average diameter ~3 μm (Fig. 1a), with a narrow size distribution. Annealing of the as-prepared sample in the reduction $P[O_2] \sim 10^{-4}$ Pa atmosphere at the moderate temperature of T = 800 °C up to nominal composition $Nd_{0.70}Ba_{0.30}MnO_{2.60}$ leads to the formation of nanometric ~100 nm grains. The appearance of the oxygen vacancies and intensive cation exchange are likely to destroy the initial grains. The nanograins combine to form a mosaic structure, which is common to the entire polycrystalline sample. The grain size determines to a some extent the properties of the crystal structure. A decrease in the grain size to the nanodimensional level is accompanied by a decrease in the unit cell volume, which is explained by an increase in the forces of surface tension relative to the bulk elastic forces [36].

The oxidation of the anion-deficient partly A-site ordered $Nd_{0.70}Ba_{0.30}MnO_{2.60}$ sample in air at the moderate temperature of T = 800 °C leads to the formation of the oxygen-stoichiometric partly A-site ordered $Nd_{0.70}Ba_{0.30}MnO_{3.00}$ (PO). The nanometric dimension of the grains (Fig. 1b) remain. The diminution of the average grain diameter leads to two competing processes: (i) the weakening of the ferromagnetic properties owing to frustration of the exchange interactions on the grain surface [37, 38] and (ii) the strengthening of the ferromagnetic properties owing to compression of the unit cell under the influence of the surface forces [39, 40]. In the extreme case the former leads to the formation of the spin glass state, while the latter leads to the increase of T_C [41].

The powder X-ray diffraction results have demonstrated that the as-prepared $Nd_{0.70}Ba_{0.30}MnO_{3.00}$ sample has an orthorhombic (SG = Imma, Z = 4) unit cell which coincides with the earlier results [42]. No additional reflections indicating a presence of impurity phases have been detected (Fig. 2a). The parameters of the unit cell for all the $Nd_{0.70}Ba_{0.30}MnO_{3.00-\delta}$ samples are collected in Table 1. The crystal structure of the overwhelming major perovskite $Nd_{0.70}Ba_{0.30}MnO_{2.60}$ phase is described in a tetragonal P4/mmm space group, peculiar to a layered ordering of $Nd^{3+}/Ba^{2+} = 1/1$ cations in the A-sublattice of the ABO_3 perovskite [28].

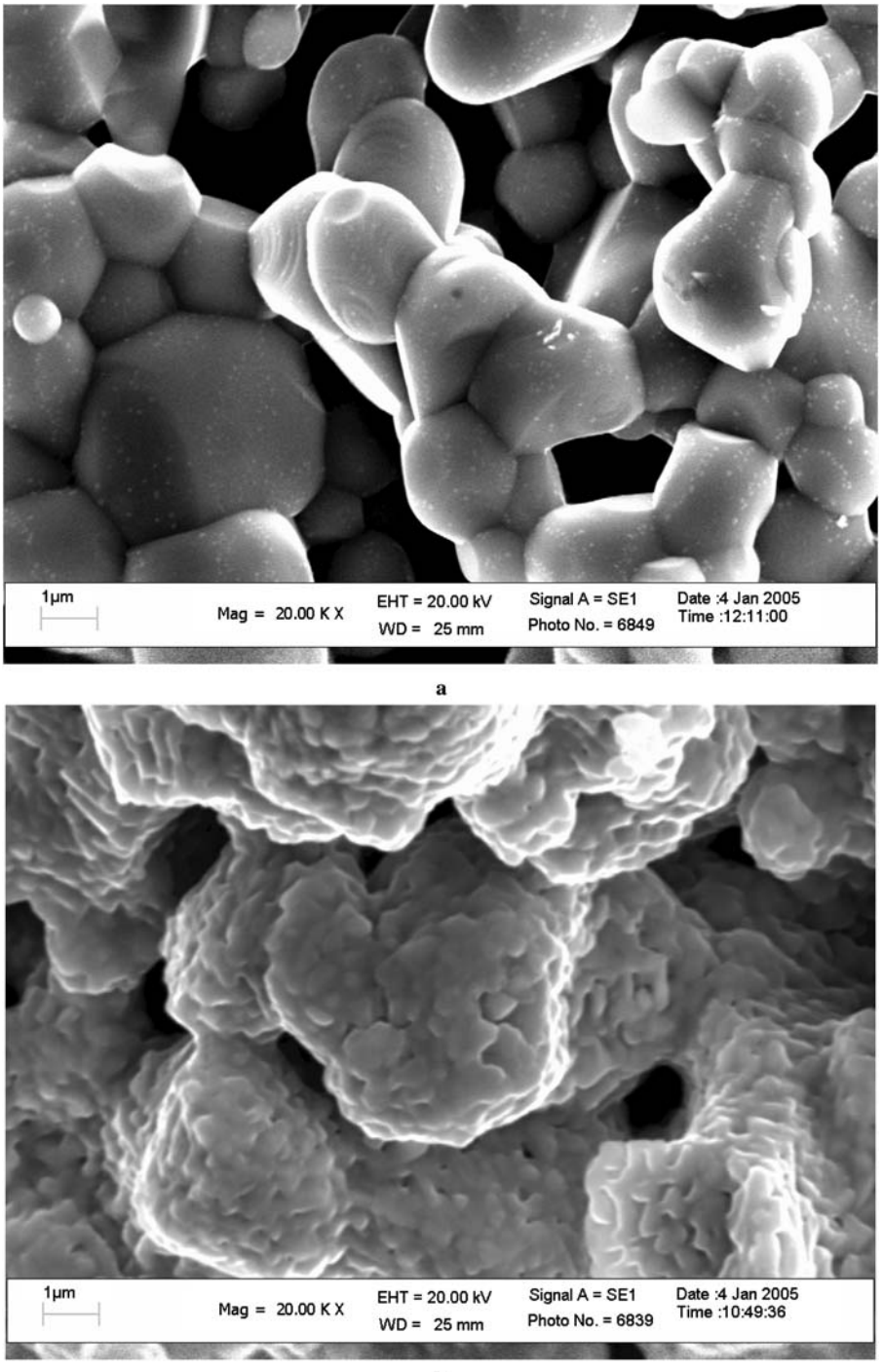

Fig. 1 The scanning electron micrographs for the as-prepared A-site disordered $Nd_{0.70}Ba_{0.30}MnO_{3.00}$ (**a**) as well as for the partly A-site ordered $Nd_{0.70}Ba_{0.30}MnO_{3.00-\delta}$ (PO) (**b**) samples

Table 1 The room-temperature unit cell parameters, ionic coordinates, bond distances and bond angles as well as error bars for the four phases of the $Nd_{0.70}Ba_{0.30}MnO_{3.00-\delta}$ samples

	$Nd_{0.70}Ba_{0.30}MnO_{3.00}$	$Nd_{1.40}Ba_{0.60}Mn_{2.00}O_{5.20}$	$NdBaMn_{2.00}O_{6.00}$	$NdMnO_{3.00+\delta}$
Space group	Imma	P4/mmm	P4/mmm	Pnma
a (Å)	5.5100(8)	3.9626(5)	3.8893(8)	5.4899(8)
b (Å)	7.7523(9)	3.9626(5)	3.8893(8)	7.7755(9)
c (Å)	5.4856(7)	7.7405(9)	7.7310(9)	5.4896(9)
V (Å^3)	234.32	243.09	233.89	234.33
Nd (x, y, z)	(0, 1/4, −0.002(3))	(0, 0, 0)	(0, 0, 0)	(0.019(3), 1/4, 0.997(3))
Ba (x, y, z)	(0, 1/4, −0.002(3))	(0, 0, 1/2)	(0, 0, 1/2)	(0.019(3), 1/4, 0.997(3))
Mn (x, y, z)	(0, 0, 1/2)	(1/2, 1/2, 0.236(2))	(1/2, 1/2, 0.245(7))	(0, 0, 1/2)
O1 (x, y, z)	(0, 1/4, 0.432(9))	(1/2, 1/2, 1/2)	(1/2, 1/2, 1/2)	(0.466(9), 1/4, 0.008(8))
O2 (x, y, z)	(3/4, −0.012(6), 1/4)	(1/2, 0, 0.195(2))	(1/2, 0, 0.230(9))	(0.216(9), 0.555(9), 0.250(9))
O3 (x, y, z)	–	–	(1/2,1/2,0)	–
⟨Mn–O1⟩ (Å)	1.973	2.044	1.974	1.953
⟨Mn–O2⟩ (Å)	1.946	2.007	1.948	1.861 + 2.122
⟨Mn–O3⟩ (Å)	–	–	1.892	–
⟨Mn–O1–Mn⟩ (°)	158.32	180.00	180.00	168.75
⟨Mn–O2–Mn⟩ (°)	174.46	161.72	173.08	154.06
⟨Mn–O3–Mn⟩ (°)	–	–	180.00	–
R_p (%)	9.01	10.11	10.31	10.31
R_{wp} (%)	13.11	14.11	14.11	14.11
R_B (%)	5.52	3.44	6.13	6.84
χ^2 (%)	2.74	2.89	2.99	2.99

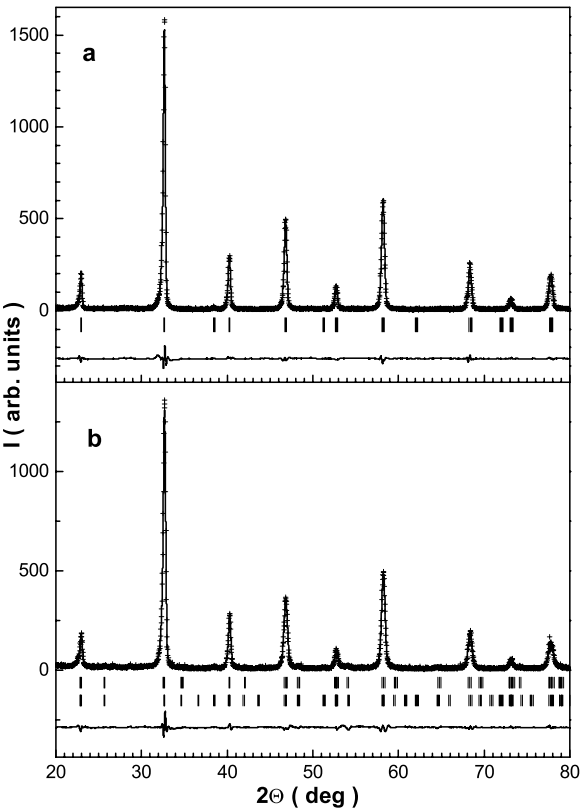

Fig. 2 The powder X-ray diffraction patterns at the room temperature for the $Nd_{0.70}Ba_{0.30}MnO_{3.00}$ manganites: (**a**) As-prepared A-site disordered, (**b**) oxidized partly A-site ordered sample. The measured data (*solid circles*) are shown together with the resulting fit (*solid line*) and their difference plot (*solid line at the bottom*). The ticks indicate the predicted 2θ positions for the Bragg peaks

The structure of the anion-deficient phase consists of pyramidal Mn^{2+}/Mn^{3+} layers, sandwiched between alternating Nd^{3+} oxygen-free and Ba^{2+} oxygen-filled layers.

The subsequent oxidation of the $Nd_{0.70}Ba_{0.30}MnO_{2.60}$ sample leads to the formation of nominally single perovskite phase with small crystal structure distortions. However the detailed examination of the diffraction spectrum of the $Nd_{0.70}Ba_{0.30}MnO_{3.00}$ (PO) sample can be represented as a superposition of the orthorhombic (SG = Pnma, Z = 4) and tetragonal (SG = P4/mmm, Z = 2) perovskite phases (Fig. 2b). The use of the Imma or Pnma one-phase mode and/or P4/mmm+Imma two-phase mode as well as the disregard of the tetragonal space group P4/mmm considerably lower the quality of the Rietveld refinement. The presence of the tetragonal group P4/mmm indicates that the cation ordering is preserved. Thus, the partly A-site ordered $Nd_{0.70}Ba_{0.30}MnO_{3.00}$ (PO) sample consists of two perovskite phases: (i) A-site ordered $NdBaMn_2O_6$ with $Nd^{3+}/Ba^{2+} = 1/1$ cation ratio and (ii) A-site disordered $NdMnO_{3+\gamma}$. The moderate T = 800 °C temperature is enough to form superstoichiometric perovskite $NdMnO_{3+\gamma}$ phase. The tetragonal symmetry is in agreement with the Nd^{3+} and Ba^{2+} cation ordering on the A-site of the perovskite cell. Of course, to be able to make a convincing statement a detailed structure refinement, possibly including also neutron diffraction, is required.

The unit cell volume of the anion-deficient A-site ordered phase is larger by ∼1% than of the as-prepared phase (Table 1). This is caused by increasing manganese ion size as result of its oxidative state decrease ($Mn^{3+} \longrightarrow Mn^{2+}$), although an oxygen vacancies and decreasing coordination number of manganese ions cause a reduction of the unit cell volume. The Mn^{3+} (HS) effective ionic radius in octahedral oxygen coordination is 0.645 Å, while in pentahedral coordination it is −0.580 Å [43]. For the Mn^{2+} (HS) ions the effective ionic radii are 0.830 Å and 0.750 Å for the octahedral and pentahedral coordination, respectively. The unit cell volume of the oxygen-stoichiometric A-site ordered phase is smaller than for the as-prepared phase. This contraction may be explained by the ordering of the A-cations and the formation of the nanograins. The grain size for the oxygen-stoichiometric A-site ordered sample is varied in region of 0.216÷0.676 μm, while for the as-prepared A-site disordered it is varied in region of 1.107 ÷ 4.606 μm. The maximal quantity of grains ∼32.91% for the oxygen-stoichiometric A-site ordered sample have size dispersion from ∼0.5 to ∼0.6 μm. Average grain size is ∼440 nm. The compression of the unit cell pro-

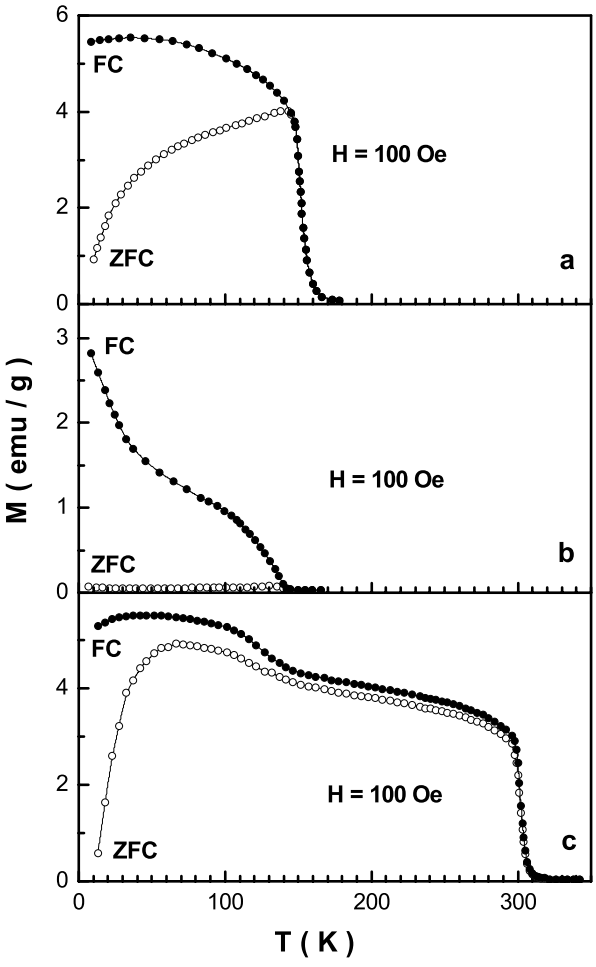

Fig. 3 The temperature dependence of ZFC (*open symbols*) and FC (*full symbols*) magnetizations in field of 100 Oe for the $Nd_{0.70}Ba_{0.30}MnO_{3.00-\delta}$ manganites: (**a**) As-prepared A-site disordered, (**b**) anion-deficient partly A-site ordered, and (**c**) oxidized partly A-site ordered sample

duces the enhancement of the exchange interactions as a result of a reduced average ⟨Mn–O⟩ bond length and increased of average ⟨Mn–O–Mn⟩ bond angle.

The results of the ZFC and FC magnetization measurements vs. temperature for the $Nd_{0.70}Ba_{0.30}MnO_{3.00-\delta}$ samples are presented in Fig. 3. The as-prepared $Nd_{0.70}Ba_{0.30}MnO_{3.00}$ sample is characterized by the Curie temperature ∼151 K (Fig. 3a). The transition to a paramagnetic state for all the samples is well defined, which is characteristic of homogeneous magnetic materials. The ZFC and FC magnetization curves for the as-prepared $Nd_{0.70}Ba_{0.30}MnO_{3.00}$ sample are very close (Fig. 3a). This indicates a small magnetic anisotropy.

The magnetic properties of the anion-deficient partly A-site ordered $Nd_{0.70}Ba_{0.30}MnO_{2.60}$ sample are due to, in general, the $NdBaMn_2O_5$ phase. The ZFC magnetization for the anion-deficient partly A-site ordered $Nd_{0.70}Ba_{0.30}MnO_{2.60}$ sample demonstrates sharp diminutive cusp at the ∼130 K. Such a type of the ZFC behavior may be attributed to antiferromagnetic or ferrimagnetic order. The ZFC and FC magnetization curves differ significantly below T_N, which is possibly due to large magnetic anisotropy. The considerable increase of the FC magnetization at the low temperatures (<20 K) seems to be caused by the Nd^{3+}-sublattice contribution.

The oxygen-stoichiometric partly A-site ordered $Nd_{0.70}Ba_{0.30}MnO_{3.00}$ (PO) sample has a Curie temperature of ∼310 K, which is more than two times as high as for the as-prepared sample (Fig. 3c). The ZFC and FC magnetization curves for the oxygen-stoichiometric partly A-site ordered $Nd_{0.70}Ba_{0.30}MnO_{3.00}$ (PO) sample are similar to the as-prepared $Nd_{0.70}Ba_{0.30}MnO_{3.00}$ (Fig. 3a,c). It is well shown that the oxygen-stoichiometric partly A-site ordered $Nd_{0.70}Ba_{0.30}MnO_{3.00}$ (PO) sample has one more magnetic transition at ∼120 K. This transition is associated with the A-site disordered $NdMnO_{3+\gamma}$ phase.

The temperature dependence of FC magnetization in a field of 10 kOe for the oxygen-stoichiometric partly A-site ordered $Nd_{0.70}Ba_{0.30}MnO_{3.00}$ (PO) sample is presented in Fig. 4. In this field the temperature of the transition to the paramagnetic state is slightly increased by ∼10 K. The transition at low temperature becomes more gradual, and the magnetization decreases slightly below ∼20 K which most probably dues to the contribution of the Nd^{3+}-sublattice. At low temperatures (<20 K) the

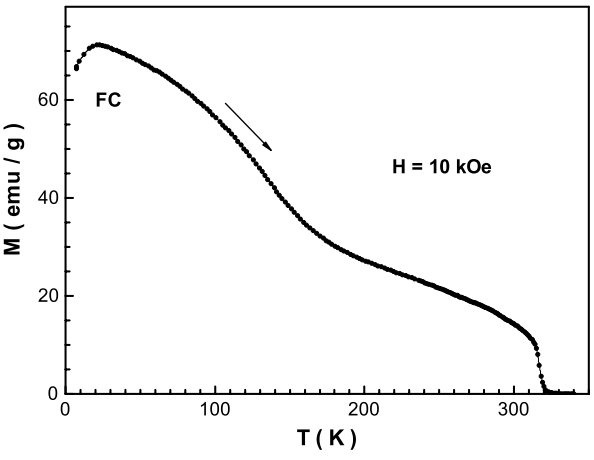

Fig. 4 The temperature dependence of FC magnetization in field of 10 kOe for the oxidized partly A-site ordered $Nd_{0.70}Ba_{0.30}MnO_{3.00}$ (PO) sample

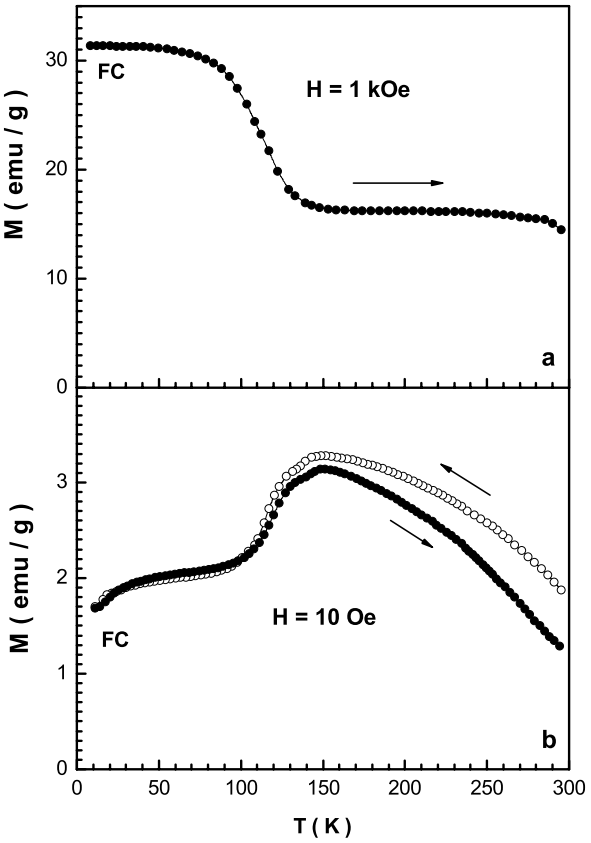

Fig. 5 The temperature dependence of FC magnetization in field of 1 kOe (**a**) and in field of 10 Oe (**b**) measured right after 1 kOe investigation for the oxidized partly A-site ordered $Nd_{0.70}Ba_{0.30}MnO_{3.00}$ (PO) sample

magnetic moments of the Nd^{3+} ions in a strong field (10 kOe) are oriented opposite to the Mn moments. One might speculate that the magnetic transitions at ∼20 K and ∼140 K are driven by structural transformations.

The two phases ($NdBaMn_2O_6$ and $NdMnO_{3+\gamma}$) of the partly A-site ordered $Nd_{0.70}Ba_{0.30}MnO_{3.00}$ (PO) sample appear to be exchange coupled. This is strongly suggested by the magnetization behavior in a weak field of 10 Oe measured immediately after the 1 kOe investigation Fig. 5. At first, the magnetization in 10 Oe increases below ∼120. After measurements in field of 1 kOe the magnetization decreases, moreover this behavior is observed for both field orientations. The high temperature magnetic phase orientes the low temperature phase. The field of 10 Oe disturbs the influence of the high temperature phase.

The field dependence of the magnetic moment for all the obtained samples at 20 K are given in Fig. 6. The as-prepared $Nd_{0.70}Ba_{0.30}MnO_{3.00}$ sample is characterized by spontaneous magnetic moment $\sigma_S \approx 3.5\ \mu_B$/f.u. that is very close to $\sigma_S \approx 3.7\ \mu_B$/f.u. which is value of moment calculated in the case of parallel orientation of manganese magnetic moments $\mu(Mn^{3+}) \approx 4\ \mu_B$ and $\mu(Mn^{4+}) \approx 3\ \mu_B$.

The anion-deficient partly A-site ordered $Nd_{0.70}Ba_{0.30}MnO_{2.60}$ sample has very small spontaneous magnetic moment in the ground state $\sigma_S \approx 0.2\ \mu_B$/f.u. Such a mo-

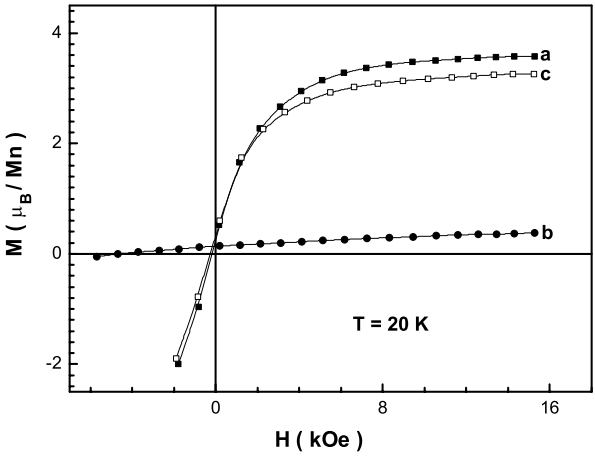

Fig. 6 The field dependence of the specific magnetic moment at the 20 K for the $Nd_{0.70}Ba_{0.30}MnO_{3.00-\delta}$ manganites: (**a**) As-prepared A-site disordered, (**b**) anion-deficient partly A-site ordered, and (**c**) oxidized partly A-site ordered phase

ment is attributed to a ferrimagnet with a small ferromagnetic component due to the incomplete compensation of antiferromagnetically ordered sublattices. A similar situation is observed for the anion-deficient A-site ordered $LBaMn_2O_5$ samples [9, 28]. If all of the $S(Mn^{2+}) = 5/2$ spins are antiparallel to the $S(Mn^{3+}) = 4/2$ spins, a saturated moment of $\sigma_S \approx 0.5\ \mu_B$ per formula unit is expected. This is comparable to the observed value of $\sim 0.2\ \mu_B$/f.u. The small moment may be also attributed to the presence of the nanodimensional grains. It should be noted the anion-deficient partly A-site ordered $Nd_{0.70}Ba_{0.30}MnO_{2.60}$ sample has large coercivity ~5.9 kOe.

After reoxidation the spontaneous magnetic moment increases up to $\sigma_S \approx 3.0\ \mu_B$/f.u. that is some lower than for the as-prepared $Nd_{0.70}Ba_{0.30}MnO_{3.00}$ sample. This fact is explained by the formation of nanograins. On the surface of grain the exchange interactions are distorted and total the magnetic moment decreases. In the case of nanograins this is especially visible. It is very likely that the small moment is also explained by the presence of nanograins in the case of the anion-deficient partly A-site ordered $Nd_{0.70}Ba_{0.30}MnO_{2.60}$ sample.

The as-prepared $Nd_{0.70}Ba_{0.30}MnO_{3.00}$ sample has an insulator type of the electrical resistivity and insulator-metal transition at ~140 K (Fig. 7a). At this temperature in field of 9 kOe the peak of magnetoresistance of ~50% is observed. The oxygen-stoichiometric A-site ordered $Nd_{0.70}Ba_{0.30}MnO_{3.00}$ (PO) sample has a Curie temperature of ~310 K, which is more than two times as large as for the as-prepared sample (Fig. 3c). The oxygen-stoichiometric partly A-site ordered $Nd_{0.70}Ba_{0.30}MnO_{3.00}$ (PO) sample has the peak of magnetoresistance of ~7% in field of 9 kOe around 310 K (Fig. 7b).

A double-exchange mechanism has been proposed by Zener to explain metallic behavior and ferromagnetic interactions in hole-doped perovskite manganites [44]. The basic process in this mechanism is played by e_g manganese electrons which move from Mn^{3+} ($t_{2g}^3 e_g^1$, S = 2) to Mn^{4+} ($t_{2g}^3 e_g^0$, S = 3/2) via the oxygen without change of the spin orientation. Thereby, Mn^{4+} and Mn^{3+} ions change places. The t_{2g}^3 electrons are always localized (giving rise to a local spin of 3/2), but the e_g electron, which is hybridized with the oxygen 2p, can be either localized or itinerant. As a

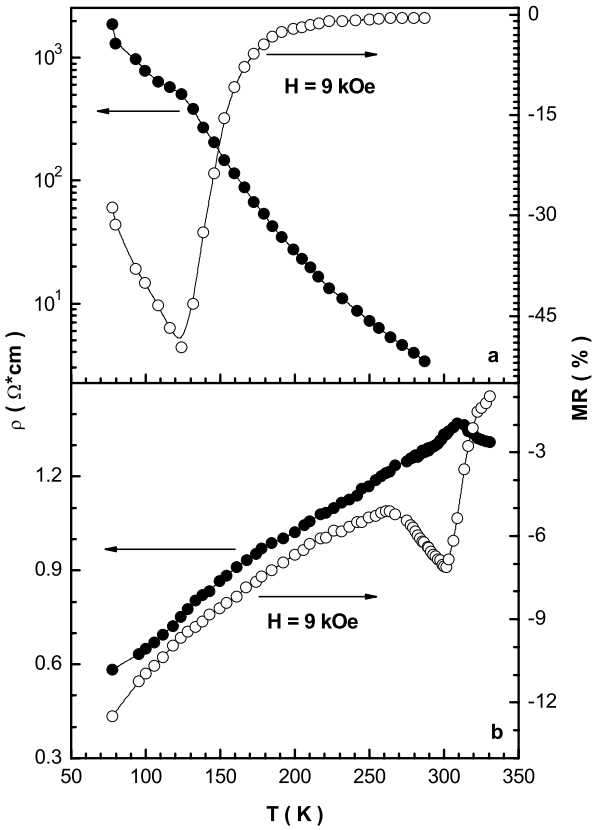

Fig. 7 The resistivity (*full symbols*) and magnetoresistance (*open symbols*) vs. temperature in field of 9 kOe for the $Nd_{0.70}Ba_{0.30}MnO_{3.00-\delta}$ manganites: (**a**) As-prepared A-site disordered, and (**b**) oxidized partly A-site ordered sample

result itinerant e_g electrons align the local spins t_{2g}^3 ferromagnetically and cause the metallic behaviour.

The magnetic state of the $L_{1-x}A_xMnO_3$ (A = Ca, Sr, Ba) manganites is known to be determined by the average radii ⟨r⟩ of alkaline-earth and rare-earth ions as well as the value of cation size mismatch $\sum x_i r_i^2 - \langle r_A \rangle^2$ in the A-sublattice which characterizes a mismatch between alkaline-earth and rare-earth ionic radii [45].

The maximum magnetic moment and Curie temperature are observed for manganites with $K = Mn^{3+}/Mn^{4+}$ equal to 7/3. If K is close to 1 the ferromagnetic state transforms into an antiferromagnetic one as the Mn^{4+} ions concentration increases. The smaller the average ionic radius of the A-sublattice and the larger the L^{3+} and A^{2+} ionic radii mismatch is the lower, in general, the magnetic ordering temperature [46].

According to the empirical Goodenough-Kanamori rules for the indirect superexchange interactions the closer the ⟨Mn–O–Mn⟩ average bond angle to 180° the larger the exchange interaction [47]. In the case of the orbitally disordered state the sign of the exchange interaction can change from positive to negative as ⟨Mn–O–Mn⟩ average bond angle decreases below a critical point. As Nd^{3+} and Ba^{2+} ions are distributed randomly on the A-sublattice the local dispersion of the Mn–O–Mn angle

value suppresses the exchange interaction value. Consequently the mismatch effect and A-site randomness weaken the ferromagnetic properties.

The ordering of cations on the A-sublattice leads to the enhancement and translation symmetry in the arrangement of the Mn–O–Mn bond angles as well as to decrease the Mn–O bond lengths (Table 1) and as a consequence to the suppression of mismatch effect. Note that the Mn–O–Mn bond angles ordering and their enhancing can also lead to a sharp increase of the magnetic ordering temperature.

The resistivity of the polycrystalline samples is determined by two contributions, i.e. contribution from the intragrain regions (grains) and contribution from the intergrain regions (grain boundaries). Spin-polarized intergrain tunneling in these compounds has been carefully studied and is known to depend on the grain size and the properties of intergranular matter, which constructs the intergrain barrier [48]. Conducting electrons can hop from grain to grain through spin-dependent tunneling. The probability of an electron tunneling with conserved spin across the intergranular barrier is reduced when the magnetic moments of the neighboring grains are not parallel. Randomly oriented moments of grains can be aligned by an external field. This causes a significant increase in the tunnel conductance, thereby reducing the resistivity of the granular sample. With grain growth, the intergranular tunneling gradually disappears, while the intragranular one is enhanced [49]. Polycrystalline manganites usually show MR effect in two distinct regions. One is pronounced near the magnetic ordering temperature (intragrain MR), the other one is dominant at low temperature where the magnetization is substantial (intergrain MR) [50]. The ordering of the cations in the A-sublattice leads to the increase the e_g-electron transfer integral inside the grains through a change in the Mn–O–Mn angle. As a result the resistivity decreases.

4 Conclusions

We investigate the A-site ordering and magnetic properties of the $Nd_{0.70}$ $Ba_{0.30}$-$MnO_{3.00}$ manganite. The high-quality ceramic with the controlled chemical phase content and microstructure has been obtained. The annealing in the reducing atmosphere $P[O_2] \sim 10^{-4}$ Pa at a moderate temperature of $T = 800\,^{\circ}C$ leads to the degradation of this ceramic and the formation of nanometric $\langle D \rangle \approx 440$ nm grains. It is shown that the partly A-site ordered manganites with $Nd^{3+}/Ba^{2+} \gg 1$ cation ratio may be obtained using a "two-steps" reduction-reoxidation method at the moderate temperature of $T = 800\,^{\circ}C$. It is observed that the A-site ordering and the formation of nanometric grains leads to considerable changes of the crystal structure and the increase of the Curie temperature. The as-prepared A-site disordered $Nd_{0.70}Ba_{0.30}MnO_{3.00}$ sample is orthorhombic (SG = Imma, Z = 4) ferromagnet below $T_C \approx 151$ K, whereas the oxidized partly A-site ordered $Nd_{0.70}Ba_{0.30}MnO_{3.00}$ (PO) sample consists from two perovskite phases: (i) A-site ordered $NdBaMn_2O_6$ one which has tetragonal (SG = P4/mmm, Z = 2) symmetry of the unit cell and Curie point ∼310 K and (ii) superstoichiometric $NdMnO_{3+\gamma}$ one which has orthorhombic (SG = Pnma, Z = 4) symmetry of the unit cell and Curie point ∼120 K. The as-prepared A-site disordered $Nd_{0.70}Ba_{0.30}MnO_{3.00}$ sample has at $T_{MI} \approx 140$ K

a peak of magnetoresistance ∼50% in field of 9 kOe. The magnetoresistance of the oxidized partly A-site ordered $Nd_{0.70}Ba_{0.30}MnO_{3.00}$ (PO) sample at the room temperature is about 7% in a field of 9 kOe. The T_C of the partly A-site ordered $Nd_{0.70}Ba_{0.30}MnO_{3.00}$ (PO) sample increases, indicating that cation order plays an important role in determining the electronic and magnetic properties not only in $Nd^{3+}/Ba^{2+} = 1/1$ materials but also in $Nd^{3+}/Ba^{2+} \gg 1$ ones. The A-site ionic ordering in $Nd_{0.70}Ba_{0.30}MnO_{3.00}$ manganite is accompanied by nanoscale chemical phase separation on the Ba-enriched and Ba-depleted regions. Two magnetic phases of the nanocomposite are exchange coupled with each other. Such considerable changes of the crystal structure and magnetic properties are interpreted in frame of the A-site ordering and the formation of nanometric grains.

Acknowledgements The work was partly supported by the Belarus Fund for Basic Research (Project F06R-078), Scholarship of the President of Republic of Belarus and the State Committee for Scientific Research (Poland) (Project KBN 1 P03B 038 27).

References

1. W. Zhou, C.T. Lin, W.Y. Liang, Adv. Mater. **5**, 735 (1993)
2. W. Zhou, Chem. Mater. **6**, 441 (1994)
3. I.O. Troyanchuk, N.V. Kasper, D.D. Khalyavin, H. Szymczak, R. Szymczak, M. Baran, Phys. Rev. Lett. **80**, 3380 (1998)
4. I.O. Troyanchuk, N.V. Kasper, D.D. Khalyavin, H. Szymczak, R. Szymczak, M. Baran, Phys. Rev. B **58**, 2418 (1998)
5. F. Millange, A. Maignan, V. Caignaert, M. Hervieu, B. Raveau, Z. Phys. B **101**, 169 (1996)
6. T.P. Beales, M. Mölgg, J. Jutson, C.M. Friend, Phys. Status Solidi A **161**, 271 (1997)
7. F. Millange, V. Caignaert, B. Domenges, B. Raveau, E. Suard, Chem. Mater. **10**, 1974 (1998)
8. A. Barnabe, F. Millange, A. Maignan, M. Hervieu, B. Raveau, G. Van Tendeloo, P. Laffez, Chem. Mater. **10**, 252 (1998)
9. J.A. McAllister, J.P. Attfield, J. Mater. Chem. **8**, 1291 (1998)
10. F. Millange, E. Suard, V. Caignaert, B. Raveau, Mater. Res. Bull. **34**, 1 (1999)
11. V. Caignaert, F. Millange, B. Domenges, B. Raveau, Chem. Mater. **11**, 930 (1999)
12. I.O. Troyanchuk, S.V. Trukhanov, H. Szymczak, K. Bärner, J. Phys.: Condens. Matter **12**, L155 (2000)
13. S.V. Trukhanov, I.O. Troyanchuk, I.M. Fita, H. Szymczak, K. Bärner, J. Magn. Magn. Mater. **237**, 276 (2001)
14. T. Nakajima, H. Kageyama, Y. Ueda, J. Phys. Chem. Solids **63**, 913 (2002)
15. S.V. Trukhanov, A.V. Trukhanov, H. Szymczak, R. Szymczak, M. Baran, J. Phys. Chem. Solids **67**, 675 (2006)
16. L. Er-Rakho, C. Michel, P. Lacorre, B. Raveau, J. Solid State Chem. **73**, 531 (1988)
17. J. Spooren, R.I. Walton, F. Millange, J. Mater. Chem. **15**, 1542 (2005)
18. A.A. Taskin, A.N. Lavrov, Y. Ando, Appl. Phys. Lett. **86**, 091910 (2005)
19. C. Perca, L. Pinsard-Gaudart, A. Daoud-Aladine, M.T. Fernandez-Diaz, J. Rodriguez-Carvajal, Chem. Mater. **17**, 1835 (2005)
20. T. Nakajima, Y.J. Ueda, J. Appl. Phys. **98**, 046108 (2005)
21. N. Furukawa, Y. Motome, J. Phys. Soc. Jpn. **74**, 203 (2005)
22. S.V. Trukhanov, L.S. Lobanovski, M.V. Bushinsky, V.V. Fedotova, I.O. Troyanchuk, A.V. Trukhanov, V.A. Ryzhov, H. Szymczak, R. Szymczak, M. Baran, J. Phys.: Condens. Matter **17**, 6495 (2005)
23. A.J. Williams, J.P. Attfield, Phys. Rev. B **72**, 024436 (2005)
24. Q. Zhang, W. Zhang, Z. Jiang, Phys. Rev. B **72**, 144415 (2005)
25. A.J. Williams, J.P. Attfield, Phys. Rev. B **72**, 184426 (2005)
26. J. Salafranca, L. Brey, Phys. Rev. B **73**, 214404 (2006)
27. S.V. Trukhanov, I.O. Troyanchuk, M. Hervieu, H. Szymczak, K. Barner, Phys. Rev. B **66**, 184424 (2002)

28. T. Nakajima, H. Yoshizawa, Y. Ueda, J. Phys. Soc. Jpn. **73**, 2283 (2004)
29. S.V. Trukhanov, JETP **101**, 513 (2005)
30. T. Nakajima, H. Kageyama, H. Yoshizawa, K. Ohoyama, Y. Ueda, J. Phys. Soc. Jpn. **72**, 3237 (2003)
31. S.V. Trukhanov, I.O. Troyanchuk, D.D. Khalyavin, I.M. Fita, H. Szymczak, K. Bärner, JETP **94**, 329 (2002)
32. T.J. Sato, J.W. Lynn, B. Dabrowski, Phys. Rev. Lett. **93**, 267204 (2004)
33. O. Chmaissem, B. Dabrowski, S. Kolesnik, J. Mais, J.D. Jorgensen, S. Short, C.E. Botez, P.W. Stephens, Phys. Rev. B **72**, 104426 (2005)
34. H.M. Rietveld, J. Appl. Crystallogr. **14**, 65 (1969)
35. J. Rodriguez-Carvajal, Physica B **192**, 55 (1993)
36. K.S. Shankar, S. Kar, G.N. Subbanna, A.K. Raychaudhuri, Solid State Commun. **129**, 479 (2004)
37. N. Zhang, W. Yang, W. Ding, D. Xing, Y. Du, Solid State Commun. **109**, 537 (1999)
38. G. Pang, X. Xu, V. Markovich, S. Avivi, O. Palchik, Y. Koltypin, G. Gorodetsky, Y. Yeshurun, H.P. Buchkremer, A. Gedanken, Mater. Res. Bull. **38**, 11 (2003)
39. K. Uchino, E. Sadanaga, T. Hirose, J. Am. Ceram. Soc. **72**, 1555 (1989)
40. S. Chattopadhyay, P. Ayyub, V.R. Palkar, A.V. Gurjar, R. Wankar, M. Multani, J. Phys.: Condens. Matter **9**, 8135 (1997)
41. S.V. Trukhanov, I.O. Troyanchuk, A.V. Trukhanov, I.M. Fita, A.N. Vasil'ev, A. Maignan, H. Szymczak, JETP Lett. **83**, 33 (2006)
42. A. Maignan, C. Martin, M. Hervieu, B. Raveau, J. Hejtmanek, Solid State Commun. **107**, 363 (1998)
43. R.D. Shannon, Acta Crystallogr. A **32**, 751 (1976)
44. C. Zener, Phys. Rev. **82**, 403 (1951)
45. L.M. Rodriguez-Martinez, J.P. Attfield, Phys. Rev. B **58**, 2426 (1998)
46. R. Mahesh, M. Itoh, Phys. Rev. B **60**, 2994 (1999)
47. J.B. Goodenough, A. Wold, R.J. Arnot, N. Menyuk, Phys. Rev. **124**, 373 (1961)
48. S.V. Trukhanov, I.O. Troyanchuk, N.V. Pushkarev, H. Szymczak, JETP **95**, 308 (2002)
49. N. Zhang, W. Ding, W. Zhong, D. Xing, Y. Du, Phys. Rev. B **56**, 8138 (1997)
50. S.V. Trukhanov, L.S. Lobanovski, M.V. Bushinsky, V.A. Khomchenko, N.V. Pushkarev, I.O. Troyanchuk, A. Maignan, D. Flahaut, H. Szymczak, R. Szymczak, Eur. Phys. J. B **42**, 51 (2004)